



or deformation [37,38] response of erythroid spectrin. However, a number of studies focusing on forced unfolding have provided insight regarding multiple intermediate regions in spectrin structure [39–43], destabilization criteria [44] and required force to disentangle spectrin filament [45,46].

### 1.3. Periodic actin-spectrin skeleton: Role in axon and high strain rate scenario

The periodicity of actin-spectrin is not only limited to the main axon, but also found in dendrites and axon initial segment [6,47–53], which is an early age phenomenon for most species [54]. While the substantiation of the periodic actin-spectrin structure and the contribution to axonal stability are significant findings [55–58], the mechanical behavior at high strain rate scenario, such as actin-spectrin separation stretch is still absent in the literature. To address such limitations, biochemical and biological approaches will dictate the actin-spectrin network studies over the next few years [59,60]. Nevertheless, the very recent mechanical studies are promising, such as the one performed on chicken dorsal root ganglion [61] depicting that axonal cytoskeletal components can provide shock-absorbing support to the axon. Such studies are paving the pathway to determine the specific contribution of actin and spectrin to the stability of the periodic network.

From the literature review, it is evident that more mechanical studies are required focusing on spectrin and actin-spectrin network, which can be achieved by computational approaches as depicted by molecular level studies on other axonal cytoskeletal components [11,62]. Keeping these aspects in consideration, this study attempts to provide novel insights regarding the specific mechanical behavior of such cytoskeletal components at extreme strain rate – which will play an instrumental role in developing a bottom-up axon model focusing on high strain rate scenario and contribute to the existent computational axon models.

## 2. Method

The required PDB file and FASTA sequence for actin and spectrin structures are obtained from RCSB and Uniprot protein data banks, and then simulation-compliant models are built based on the predicted structures obtained from the i-TASSER predictor software [63]. The reason of proceeding with i-TASSER predicted structure is its reliability quantified by CASP and recent successful implementation of predicted structure in MD simulations [11,64,65].

The PDB files are converted into LAMMPS [66] readable data files that implements OPLS force field [67,68] for simulation. The simulation box is filled with explicit water molecules, for which

MARTINI force field [69] is used for van der Waals interaction parameters. Required Na<sup>+</sup> and Cl<sup>-</sup> ions were added to obtain charge neutralization for explicit solvent simulations.

The general scheme of the simulation comprises of:

- Minimizing potential energy at 310 K (the flat potential energy vs time graph ensures well equilibration),
- Using inner and outer cutoff of LJ potentials as 10 and 12, respectively,
- Using solver pppm (particle-particle particle-mesh), which facilitates the computation of long-range coulombic interaction,
- NVT equilibration of the system with 100 fs temperature damping parameter (first 100 ps),
- NPT equilibration of the system with target pressure of 1 bar (for another 100 ps),
- Performing tensile tests by pulling the residues along the length axis, towards the opposite direction, at the strain rates of  $10^8 \text{ s}^{-1}$  and  $10^9 \text{ s}^{-1}$  [62]. It is assumed that ~0% of strain is sufficient to obtain the stiffness data.

Table 1 summarizes the box size of the systems and the specific tensile test schemes.

### 2.1. Tensile test on 6-actin and 12-actin models

To determine mechanical property of actin, 6-actin and 12-actin models are utilized. Both models are built from existent literature. The 6-actin model is obtained from “actin filament pointed end” structure found by electron microscopy deposited with PDB ID 2Y83 [70], while the 12-actin model is obtained from the cryo-EM structure of actin deposited with PDB ID 3G37 [71]. The objective of tensile test is to observe strain rate dependence and difference between the stretching mechanism between short and long F-actin filaments.

### 2.2. Tensile test on $\alpha$ -spectrin and $\beta$ -spectrin

For  $\alpha$ -spectrin and  $\beta$ -spectrin, the models are built from Uniprot structures – for non-erythrocytic  $\alpha$ -spectrin (gene: SPTAN1) [72] and  $\beta$ -spectrin (SPTBN2) [73] structures. These sources facilitate specification of domains and repeat regions, which is utilized in the modeling and tensile tests. The tensile test scheme is similar to that of actin. The simulation-compliant versions are created by using the last seven (7) repeats and the EF hand regions for  $\alpha$ -spectrin, while the first seven (7) repeats and the actin binding domain are used for  $\beta$ -spectrin. According to the comprehensive

**Table 1**  
Simulation setup for tensile tests on actin, spectrin, and actin-spectrin models.

System	Simulation Box Size (nm × nm × nm) [Note: biggest dimension is always in the length (or pulling) direction]	Number of protein atoms	Number of atoms in the system (approx. in millions)	Boundary Condition or Loading Scheme for Tensile Test (all are performed for strain rates $1 \times 10^8 \text{ s}^{-1}$ and $1 \times 10^9 \text{ s}^{-1}$ )
6 Actin	13 × 13 × 48.5	35,202	0.75	First 100 and last 100 residues are pulled towards the opposite direction
12 Actin	17 × 17 × 63.5	70,548	1.6	First 100 and last 100 residues are pulled towards the opposite direction
$\alpha$ -Spectrin	68.5 × 12 × 12	13,034	0.9	Left-most repeat region is pulled towards -x direction, right-most repeat region and EF regions are pulled towards + x direction
$\beta$ -Spectrin	68 × 12 × 12	15,342	0.9	Left-most repeat region and actin-binding region are pulled towards -x direction, right-most repeat region is pulled towards + x direction
Actin-Spectrin	58 × 11 × 38.5	87,702	2.2	The outermost 50 residues of the two $\beta$ -Spectrins attached to the 12-actin surface are pulled towards the opposite directions

review study on spectrin [7], 19–20 repeats in  $\alpha$ -spectrin and 1–2 repeats in  $\beta$ -spectrin are sufficient for actin-spectrin modeling, and therefore, it is ensured that these repeats are included in the standalone spectrin models. The specification of the residue numbers of both spectrin isoforms are provided in Table 1. Aside from obtaining the mechanical property, another objective of the tensile test on standalone spectrin is to observe the unfolding mechanism.

### 2.3. Determination of actin-spectrin interaction

For actin-spectrin interaction model, two  $\beta$ -spectrin filaments (a smaller version with the actin-binding domain and the first two repeats) [7] are attached to the 12-actin surface, and then pulled at the opposite directions. The objective of applying two different strain rates is to observe the strain rate dependence and possible separation mechanism. This ensures that possible high strain rate scenarios are covered where either of the axonal cytoskeletal components might be susceptible to stretching.

### 2.4. Stress-strain calculation and tensile test schemes

Calculation of the stress and strain are similar to recently published MD work on axonal cytoskeletal component of neuron [11].

In a simple manner, the stress-strain calculation scheme can be pointed out as:

- Obtaining stress values from per-atomic stress tensor in LAMMPS, which is associated with the volume of the respective group of atoms,
- Calculating approximate volume of the group of atoms by implementing Voronoi feature of LAMMPS, which is included in the voro++ package,
- Dividing the (stress  $\times$  volume) data by the approximate volume from Voronoi calculation to obtain the stress data,
- Obtaining strain values from displacement data of atoms [74],
- Maintaining NVT ensemble throughout the tensile test, with a 100 fs temperature damping parameter.

As a relevant note, visualization snapshots are obtained by OVITO [75]. All the simulations were carried out by the STAMPEDE2 and Lonestar supercomputers of Texas Advanced Computing Center (TACC).

## 3. Results

### 3.1. Mechanical behavior of actin

For 6-actin and 12-actin systems, uniaxial tensile tests are performed at two strain rates,  $10^8 \text{ s}^{-1}$  and  $10^9 \text{ s}^{-1}$ . Figs. 1–3 show the stress-strain response and tensile test snapshots for the 6-actin system, while Figs. 4–6 show the same for the 12-actin system. It is observed that both 6-actin and 12-actin behave as stiffer material at higher strain rate. However, the stretching stiffness is in the range found in the literature, even at such high strain rate.

### 3.2. Mechanical behavior of spectrin

For  $\alpha$ -spectrin and  $\beta$ -spectrin systems, uniaxial tensile tests are performed at two strain rates,  $10^8 \text{ s}^{-1}$  and  $10^9 \text{ s}^{-1}$ . Figs. 7–9 show the stress-strain response and tensile test snapshots for the  $\alpha$ -spectrin system, while Figs. 10–12 show the same for the  $\beta$ -actin system. It is observed that spectrin also behaves as stiffer material when susceptible to higher strain rate. However, the extent of dependence on the strain rate is relatively lower, as spectrin goes through unfolding stage of the interrepeat domains unlike actins (which manifest stretching of the F-actin filaments even at low strain due to strong bond between G-actins in the filament) as depicted by the snapshots.

Table 2 summarizes the stiffness result based on the linear fit of 10% strain vs stress data of actin and spectrin models.

### 3.3. Actin-spectrin interaction

For actin-spectrin systems, tensile tests are performed at two strain rates,  $10^8 \text{ s}^{-1}$  and  $10^9 \text{ s}^{-1}$  by attaching two  $\beta$ -spectrin to the surface of a 12-actin system, and then pulled away towards the opposite directions. Figs. 13 and 14 show the tensile test snapshots for the system for  $10^8 \text{ s}^{-1}$  and  $10^9 \text{ s}^{-1}$ , respectively. It is depicted that not only the separation differs according to the applied strain rate, but also the failure mechanism. At lower strain rate, the prone-to-failure region is the actin-spectrin interface, while at higher strain rate, it is the inter-repeat regions of spectrin.

## 4. Discussion

The tensile tests performed in this study provides novel insights into mechanical behavior of actin, spectrin, and actin-spectrin cytoskeleton in axon. However, as a computational study, some common issues must be addressed – such as selection of force field, application of strain rate, and using predicted structure for protein.

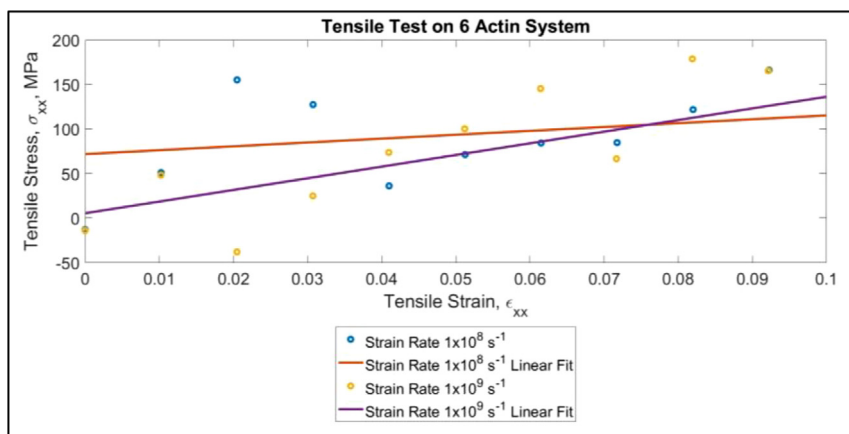


Fig. 1. Stress-strain response of 6 actin system for two strain rates.



**Fig. 2.** Snapshots of tensile test on 6-actin system at strain rate  $1 \times 10^8 \text{ s}^{-1}$ . Strain: a) 0%, b) 5%, c) 10%. The atoms being pulled are shown in red color. For the rest, the default coloring of OVITO software is retained. (For interpretation of the references to color in this figure legend, the reader is referred to the web version of this article.)

First, selection of appropriate force field is vital for realistic representation of a biophysical scenario. In this study, OPLS force field is used for simulations, as it is specifically fine-tuned for protein simulation [76,77]. Recently it is found that non-reactive force field such as CHARMM can successfully capture high deformation phenomena for cytoskeletal components of neuron [11,62]. As a benchmark test, the tensile test on  $\alpha$ -spectrin is performed for both CHARMM and OPLS force fields, which shows comparable results as depicted in the Appendix 1.

Second, the strain rates used in this study for the tensile tests fall into “extreme” range for axonal cytoskeletal components. However, recent computational study on such components has found such range of strain rates as relevant to cavitation bubble implosion (blast-induced traumatic brain injury (TBI) scenario) [62].

And third, proceeding with predicted structure obtained from the FASTA sequence available in the protein data bank (PDB) is justified due to increased application and successful implementation in the recent years [11,64,65,78].

In the following sub-sections, the specific aspects of the obtained results, their impact, and future directions are discussed.

#### 4.1. Mechanical behavior of actin in high strain rate scenario

Studies that explored the failure mechanism of actin have emphasized the effect of actin-severing proteins, such as cofilin [27,79]. While it is admitted that both biochemical and mechanical aspects should be considered for determining mechanical behavior of actin at high strain rate, it can be argued that effect of mechanical loading (applied tension on the protein in this study) will be most significant at extreme strain rate scenario, which is shown in recent studies on other axonal cytoskeletal components of neuron [11,62]. Furthermore, from the results of both 6-actin and 12-actin systems it is substantiated that actin behaves as a stiffer material at higher strain rate. Increase of extensional and torsional stiffness is established in the literature [14], which is in harmony with the finding of the current study. Therefore, from the perspective of extensional stiffness, it can be asserted that mechanical behavior of actin is maintained throughout a large range of tensile

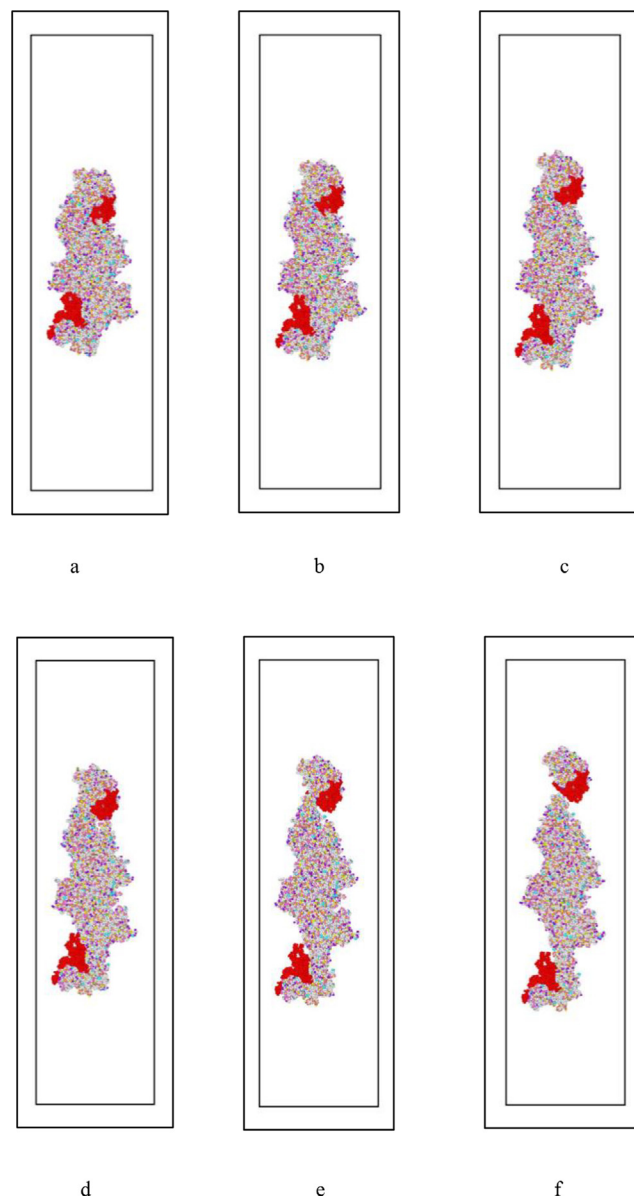


**Fig. 3.** Snapshots of tensile test on 6-actin system at strain rate  $1 \times 10^9 \text{ s}^{-1}$ . Strain: a) 0%, b) 10%, c) 20%, d) 30%, e) 40%, f) 50%. The onset of failure is found at  $\sim 30\%$  strain, where for complete failure (fragmentation of the main filament) occurs at  $\sim 50\%$ . The atoms being pulled are shown in red color. For the rest, the default coloring of OVITO software is retained. (For interpretation of the references to color in this figure legend, the reader is referred to the web version of this article.)

loading. The only difference between the 6-actin and 12-actin system is the failure mechanism. For 6-actin or shorter system, actin tends to fail along the junction of G-actin to G-actin. Similar type of failure is also observed for MTs at extreme strain rate, which fails along the line of the tubulin junction when susceptible to tensile loading [62]. As there is mainly electrostatic and van der Waals bond i.e. non-bonded interactions between G-actins, it is expected that these bonds will be broken before the covalent bonds within the G-actin atoms. However, for longer system (12-actin), the pulled region is substantially smaller than the overall filament length, and therefore, the tensile load can be carried along the length of the whole filament – leading to high stretchability. The range of stiffness is, however, coherent with recent review work [10], which suggests that at high strain rate, actin stiffness will be at the high end of the range proposed (400 MPa–2.5GPa) [14–19,32].

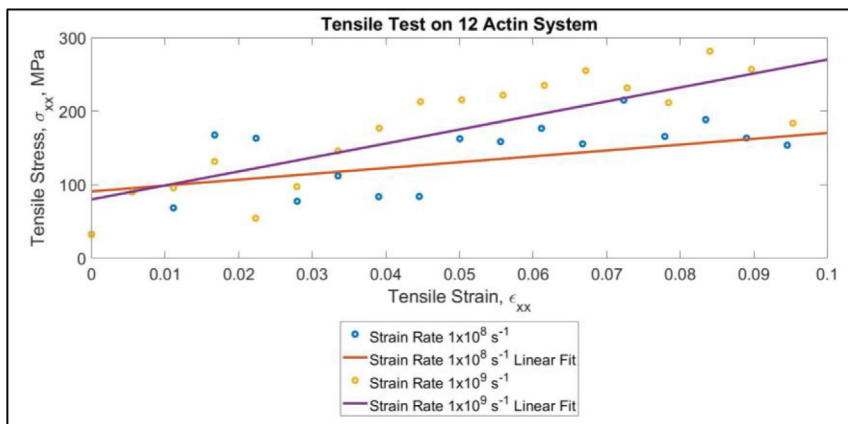


Fig. 4. Stress–strain response of 12 actin system for two strain rates.

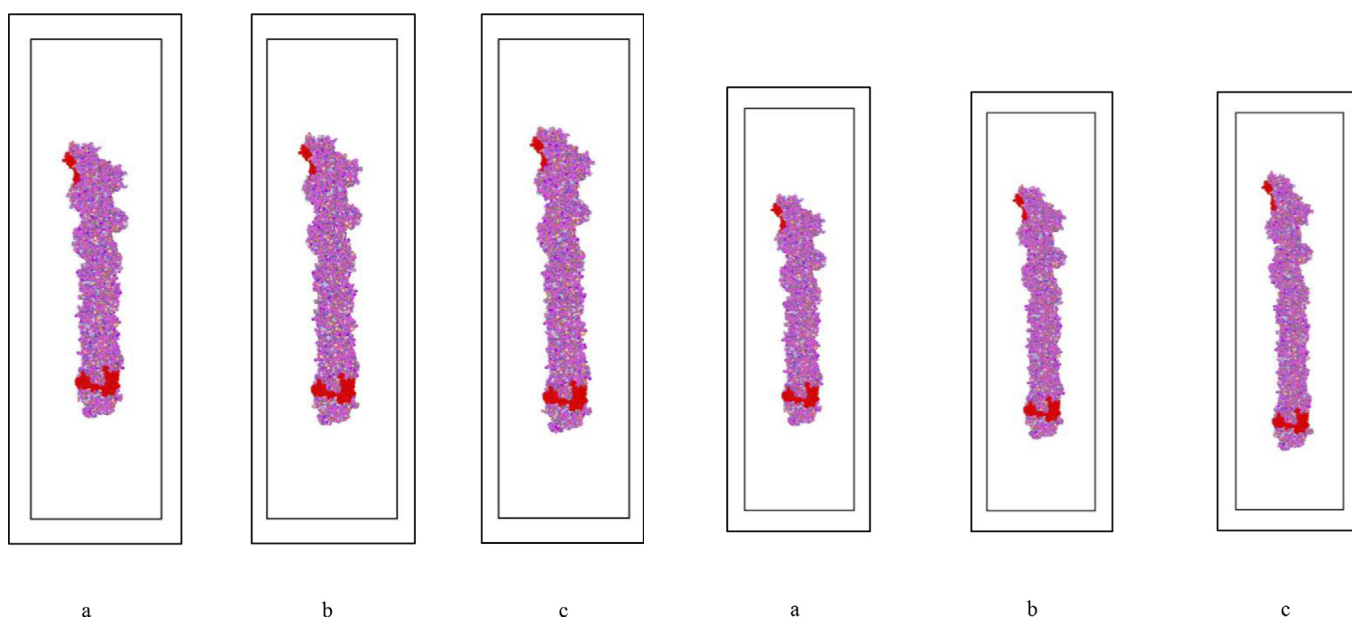


Fig. 5. Snapshots of tensile test on 12-actin system at strain rate  $1 \times 10^8 \text{ s}^{-1}$ . Strain: a) 0%, b) 5%, c) 10%. The atoms being pulled are shown in red color. For the rest, the default coloring of OVITO software is retained. (For interpretation of the references to color in this figure legend, the reader is referred to the web version of this article.)

4.2. Mechanical behavior of spectrin in high strain rate scenario

Similar to that of actin, the mechanical behavior of spectrin can also be explained from the biochemical perspective [34]. Earlier atomic force microscopy (AFM) studies on spectrin tandem repeats and single spectrin have established that susceptibility to tensile loading leads to unfolding and stretching, which is impressively close to the observation in the current study [39,40,42]. Furthermore, the high stretchability can be attributed to the initial “folded” state of the repeat regions and the inter-repeat regions, which get unfolded due to applied high strain rate. Although the force required to unfold spectrin has been found to be small [45], it can be asserted that due to having multiple un-foldable regions throughout the structure, axonal spectrin can have high stretchability. However, the multiple fold is attributed to the mechanical strength of the spectrin filament, and unfolding leads to vulnerability to failure. It is discussed in recent studies that axonal cytoskeletal components provide mechanical stretchability due to their

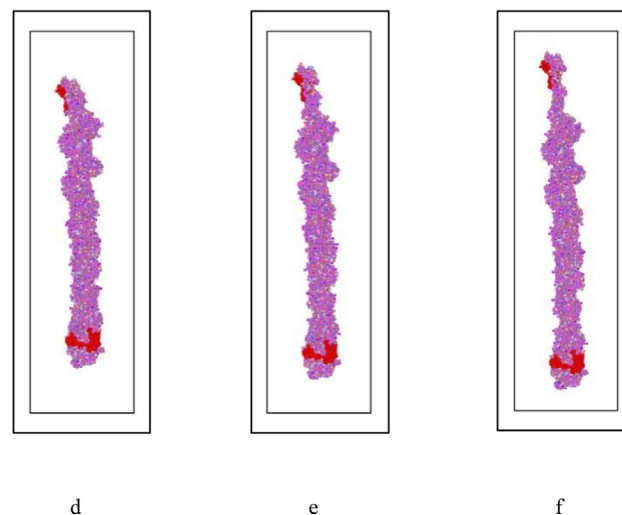


Fig. 6. Snapshots of tensile test on 12-actin system at strain rate  $1 \times 10^9 \text{ s}^{-1}$ . Strain: a) 0%, b) 10%, c) 20%, d) 30%, e) 40%, f) 50%. This longer filament does not show failure by fragmentation, rather it shows increased stretchability. The atoms being pulled are shown in red color. For the rest, the default coloring of OVITO software is retained. (For interpretation of the references to color in this figure legend, the reader is referred to the web version of this article.)

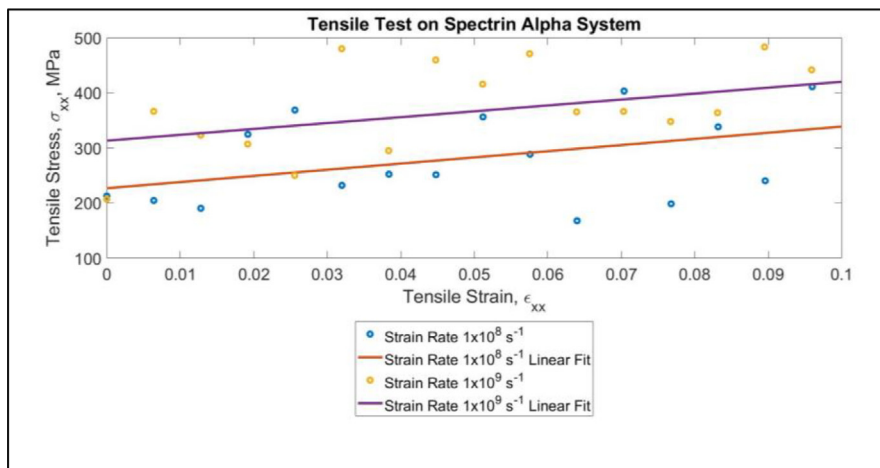


Fig. 7. Stress–strain response of  $\alpha$ -spectrin system for two strain rates.

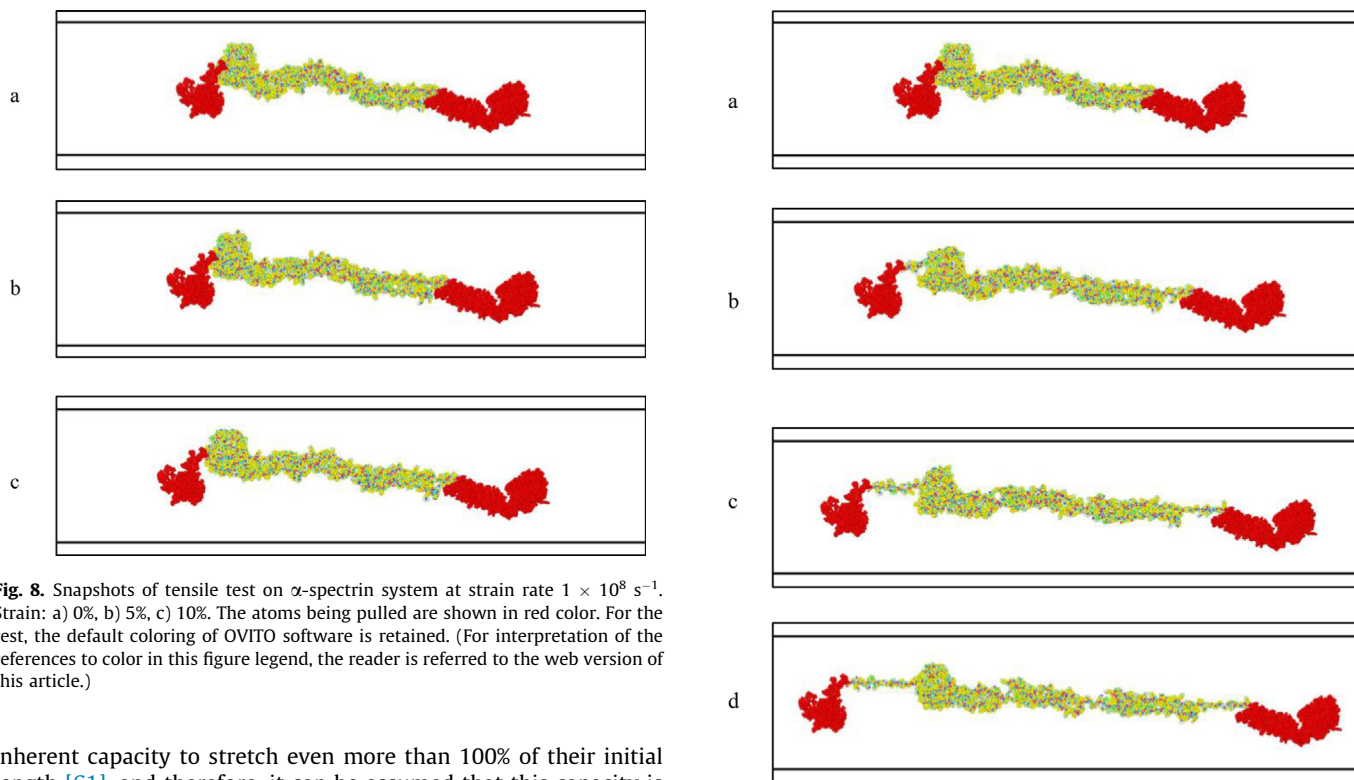


Fig. 8. Snapshots of tensile test on  $\alpha$ -spectrin system at strain rate  $1 \times 10^8 \text{ s}^{-1}$ . Strain: a) 0%, b) 5%, c) 10%. The atoms being pulled are shown in red color. For the rest, the default coloring of OVITO software is retained. (For interpretation of the references to color in this figure legend, the reader is referred to the web version of this article.)

Fig. 9. Snapshots of tensile test on  $\alpha$ -spectrin system at strain rate  $1 \times 10^9 \text{ s}^{-1}$ . Strain: a) 0%, b) 20%, c) 40%, d) 60%. The unfolding of the inter-repeat domains are manifested strongly at high strain rate. The atoms being pulled are shown in red color. For the rest, the default coloring of OVITO software is retained. (For interpretation of the references to color in this figure legend, the reader is referred to the web version of this article.)

inherent capacity to stretch even more than 100% of their initial length [61], and therefore, it can be assumed that this capacity is originated from the ability of membrane-associated proteins in axon which contain folded regions i.e. spectrins. Therefore, the results on spectrin not only substantiates the structural and mechanical insights present in the current literature, but also provides indirect causation of the ability of axon to stretch significantly.

#### 4.3. Actin-Spectrin interaction in high strain rate scenario

There is little insight present in the current literature regarding actin-spectrin network [61]. From the actin-spectrin models in the current study it is substantiated that even at high strain rate, actin-spectrin lattice can provide substantial mechanical support. Also, two different manners of failure can be observed according to the applied strain rates. At lower strain rate, there is significant stretch in spectrin, but the primary failure-prone region is the actin-spectrin interface. However, the scenario is different at

higher strain rate, as the tensile loading gets less amount of time to be propagated through the spectrin filament and manifested at the interface region. Therefore, it is observed that the more damage-prone area is the inter-repeat regions of spectrin – same observation obtained in standalone spectrin tensile tests performed in this study. In other words, at a high strain rate scenario, there could be occurrence of different failure along the periodic actin-spectrin lattice: such as separation of spectrin from actin surface, substantial spectrin unfolding, or both. In any case, the result is disorientation of the axonal cytoskeleton of neuron, regarding

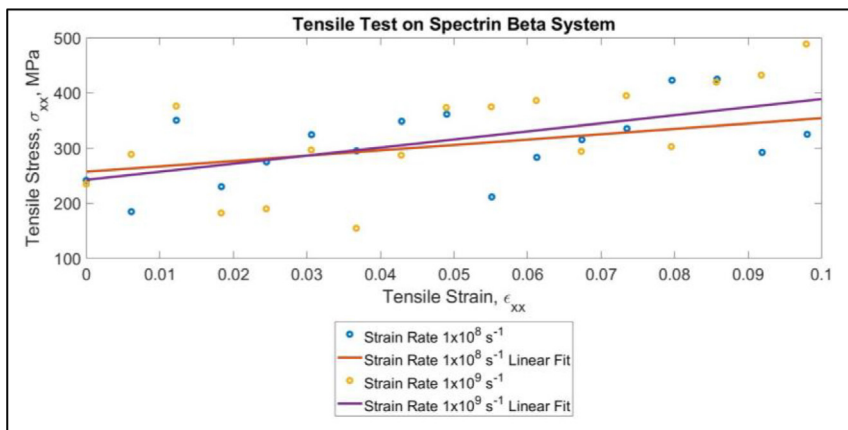


Fig. 10. Stress–strain response of  $\beta$ -spectrin system for two strain rates.

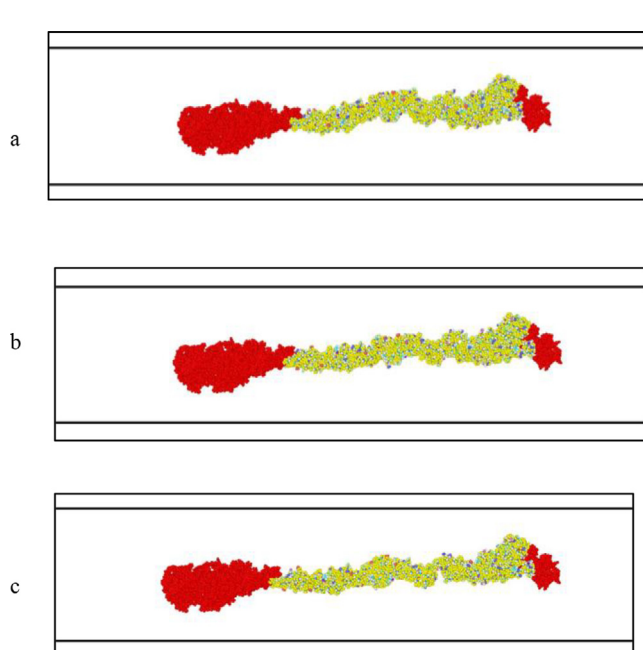


Fig. 11. Snapshots of tensile test on  $\beta$ -spectrin system at strain rate  $1 \times 10^8 \text{ s}^{-1}$ . Strain: a) 0%, b) 5%, c) 10%. The atoms being pulled are shown in red color. For the rest, the default coloring of OVITO software is retained. (For interpretation of the references to color in this figure legend, the reader is referred to the web version of this article.)

which this study provides a novel, strictly mechanical insight from high strain rate perspective. However, for more comprehensive insight, length-dependent tests could also be performed as the F-actin models in this study. For this purpose, different number of repeats might be implemented in the actin-spectrin models. Optimistically, the future works will be considering coarse-grained models to accommodate longer filament lengths and multiscale approach to obtain lattice-level mechanical response.

### 5. Conclusion

In this study, mechanical behavior of actin, spectrin, and actin-spectrin interaction at high strain rate are determined. The major findings can be summarized as below:

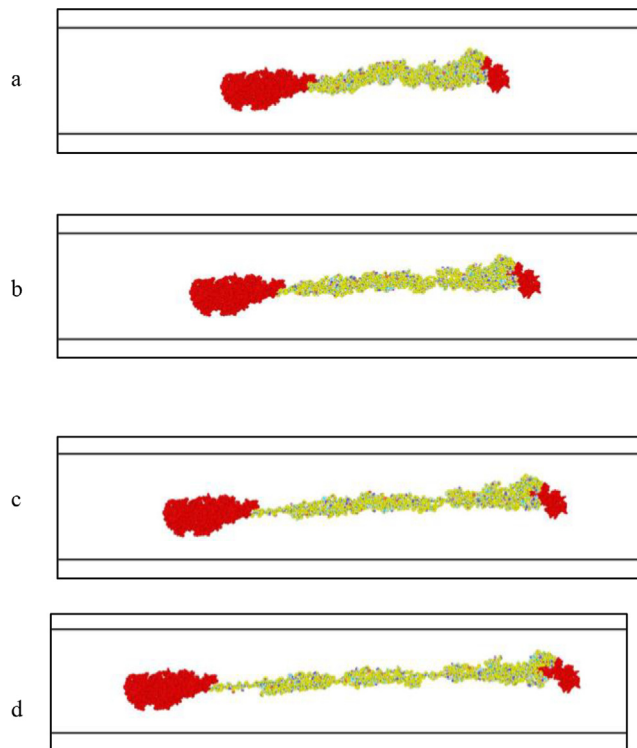
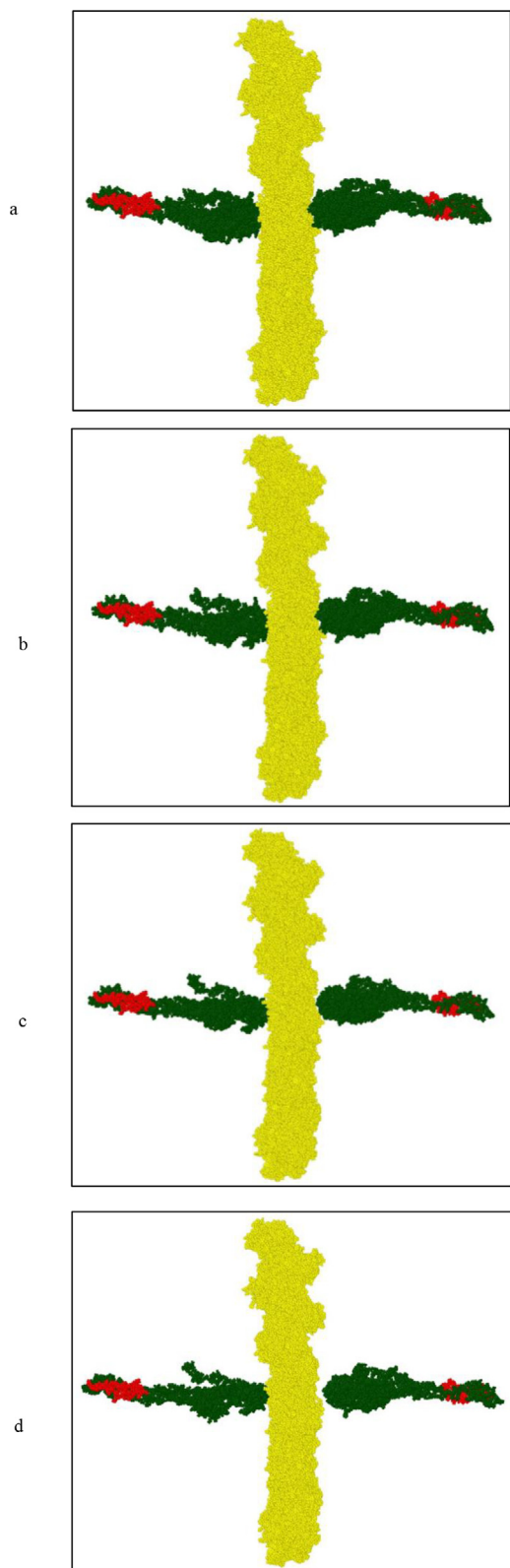


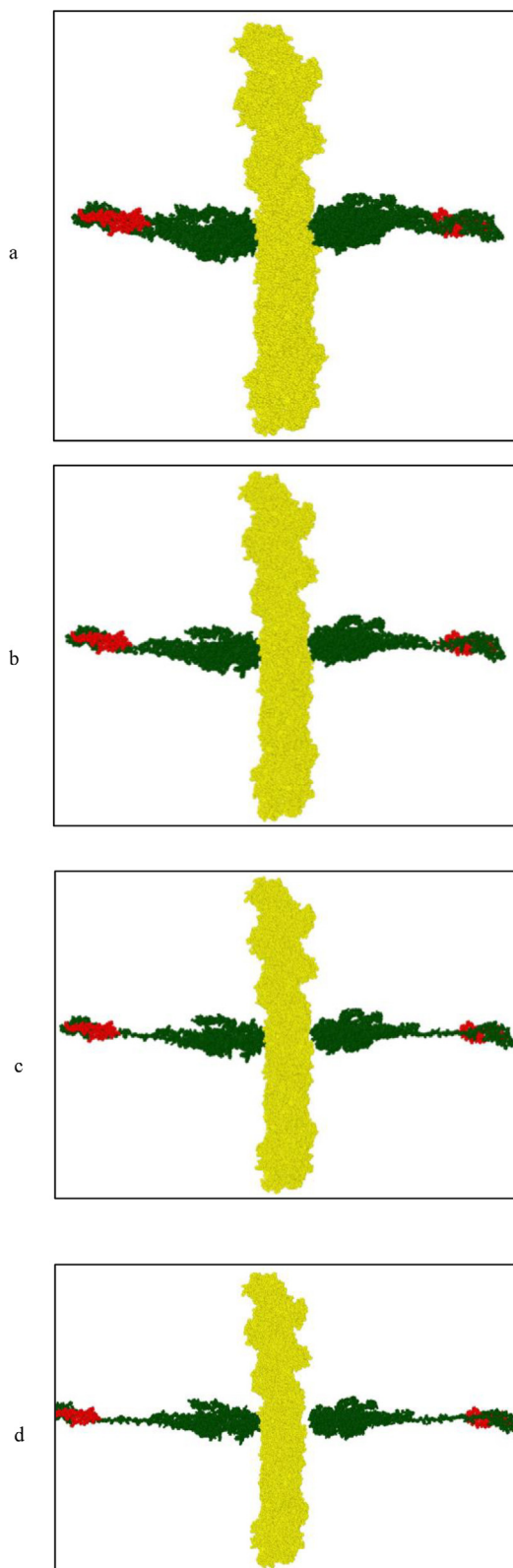
Fig. 12. Snapshots of tensile test on  $\beta$ -spectrin system at strain rate  $1 \times 10^9 \text{ s}^{-1}$ . Strain: a) 0%, b) 20%, c) 40%, d) 60%. The unfolding of the inter-repeat domains is manifested strongly at high strain rate. The atoms being pulled are shown in red color. For the rest, the default coloring of OVITO software is retained. (For interpretation of the references to color in this figure legend, the reader is referred to the web version of this article.)

Table 2  
Stiffness summary from the tensile tests on actin and spectrin models.

Model	Stiffness (MPa)	
	$1 \times 10^8 \text{ s}^{-1}$	$1 \times 10^9 \text{ s}^{-1}$
12-actin	919	2054
6-actin	852	1816
Spectrin- $\alpha$	973	2107
Spectrin- $\beta$	1120	1067



**Fig. 13.** Actin-spectrin interaction at strain rate  $1 \times 10^8 \text{ s}^{-1}$ . a) 0%: initial, b) 6%: stretching of  $\beta$ -spectrin, c) 12.5%: onset of separation, d) 18.75%: complete separation. Legend: Yellow: 12-actin, Green:  $\beta$ -spectrin, Red: atoms being pulled. (For interpretation of the references to color in this figure legend, the reader is referred to the web version of this article.)



**Fig. 14.** Actin-spectrin interaction at strain rate  $1 \times 10^9 \text{ s}^{-1}$ . a) 0%: initial, b) 23.5%: stretching and unfolding of  $\beta$ -spectrin, c) 42.3%: onset of separation, d) 58.75%: complete separation. Legend: Yellow: 12-actin, Green:  $\beta$ -spectrin, Red: atoms being pulled. (For interpretation of the references to color in this figure legend, the reader is referred to the web version of this article.)

- Actin: Both short and long F-actin filaments show stiffer characteristics at higher strain rate. Short filament tends to fail at the G-actin to G-actin junction, while long filament shows increased stretchability.
- Spectrin: Both  $\alpha$ -spectrin and  $\beta$ -spectrin show high stretchability. Unfolding of inter-repeat regions is strongly manifested at higher strain rate.
- Actin-spectrin: Failure occurs at actin-spectrin interface at lower strain rate, while significant unfolding of spectrin occurs at higher strain rate.

This study not only substantiates recent findings on periodic axonal structure of cytoskeleton, but also provides novel insights regarding the mechanical behavior and interaction. Therefore, this study will provide pathway for bottom-up axon modeling, contribute to refinement of existent computational axon models, and invoke further research focusing on high strain rate scenario.

### Author contributions

M.I.K. performed prediction of the structures, ran the simulations, interpreted the results, and wrote the manuscript. S.F. made and optimized all the models of actin and spectrin. A.A. designed the study and revised the manuscript. All the authors reviewed the manuscript.

### Declaration of Competing Interest

The authors declare that they have no known competing financial interests or personal relationships that could have appeared to influence the work reported in this paper.

### Acknowledgements

This work has been funded by the Computational Cellular Biology of Blast (C2B2) program through the Office of Naval Research (ONR) (Award No. N00014-18-1-2082- Dr. Timothy Bentley, Pro-

gram Manager). The authors acknowledge the Texas Advanced Computing Center (TACC) at The University of Texas at Austin for providing HPC resources that have contributed to the research results reported within this paper. URL: <http://www.tacc.utexas.edu>.

## Appendix A

### Appendix 1. Comparison between CHARMM and OPLS force field results: Tensile test on $\alpha$ -spectrin

To compare CHARMM with respect to OPLS, two identical models are created for  $\alpha$ -spectrin, and the tensile test is performed at strain rate  $1 \times 10^8 \text{ s}^{-1}$  as per the “Method” section in this manuscript. Fig. A1 shows the stress-strain response for both force fields, which depicts that both force fields similar results. Furthermore, Fig. A2 shows that both CHARMM and OPLS shows similar manner of unfolding in  $\alpha$ -spectrin. Considering these findings, it can be concluded that both force fields are equally eligible candidates for such simulations.

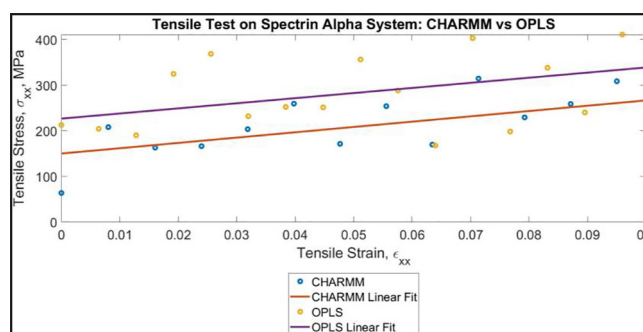


**Fig. A1.** Comparison between CHARMM and OPLS tensile test results for  $\alpha$ -spectrin. For CHARMM, the stiffness is 1164 MPa, while for OPLS, it is 1120 MPa.

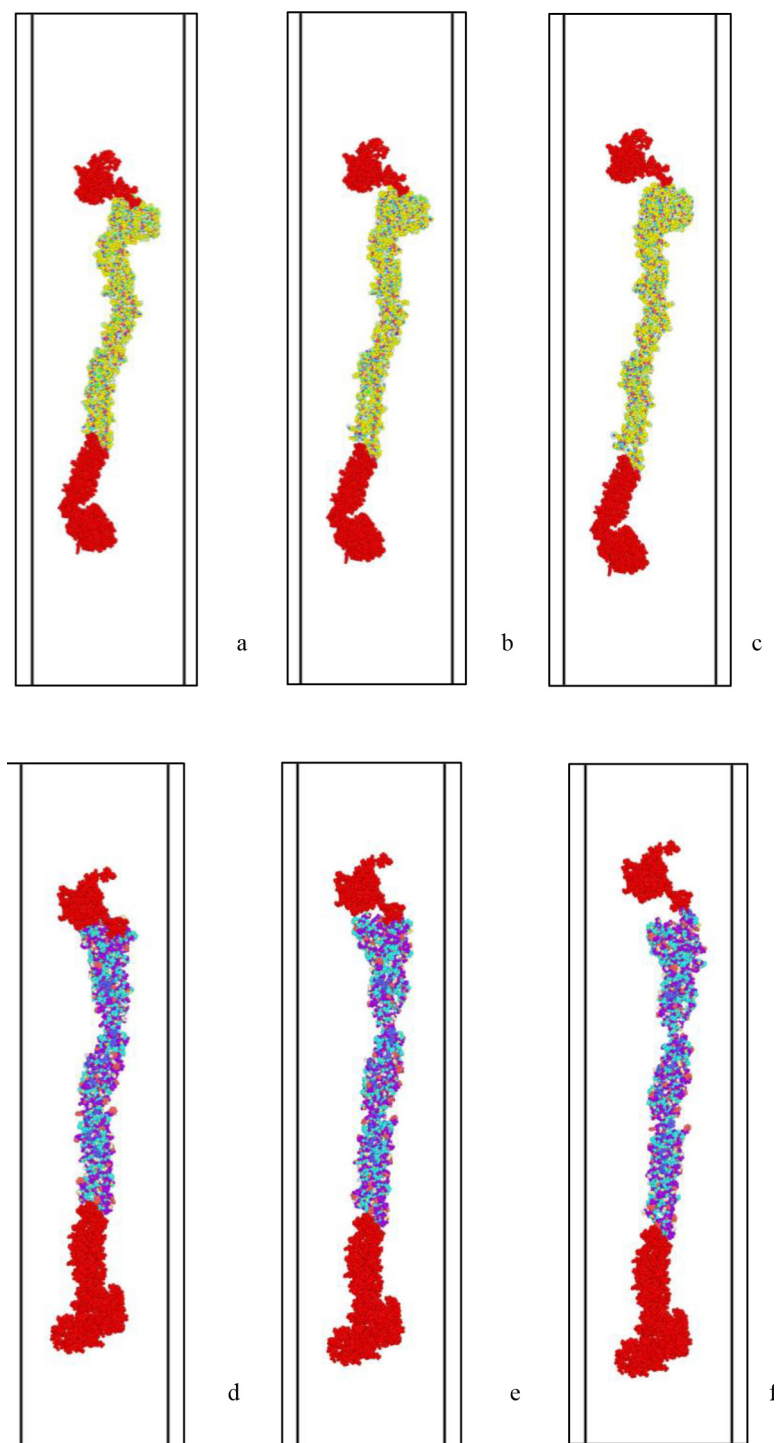


**Fig. A2.** Tensile test snapshots at 0%, 5%, and 10% strain for  $\alpha$ -spectrin created by a-c) OPLS, d-f) CHARMM. Atoms being pulled are shown in red color. For the rest, the default coloring by OVITO is retained.

## References

- [1] Avila J. Microtubule dynamics. *FASEB J* 1990;4(15):3284–90. <https://doi.org/10.1096/fsb2.v4.1510.1096/fasebj.4.15.2253844>.
- [2] Rosenberg KJ, Ross JL, Feinstein HE, Feinstein SC, Israelachvili J. Complementary dimerization of microtubule-associated tau protein: Implications for microtubule bundling and tau-mediated pathogenesis. *Proc Natl Acad Sci* 2008;105(21):7445–50.
- [3] Lee G, Neve RL, Kosik KS. The microtubule binding domain of tau protein. *Neuron*. 1989. 2. 1615–24. [https://doi.org/10.1016/0896-6273\(89\)90050-0](https://doi.org/10.1016/0896-6273(89)90050-0).
- [4] Janmey PA, Letierrier J-F, Herrmann H. Assembly and structure of neurofilaments. *Curr Opin Colloid Interface Sci* 2003;8(1):40–7.
- [5] Ouyang H, Nauman E, Shi R. Contribution of cytoskeletal elements to the axonal mechanical properties. *J Biol Eng*. 2013;7(1):21. <https://doi.org/10.1186/1754-1611-7-21>.
- [6] Xu K, Zhong G, Zhuang X. spectrin, and associated proteins form a periodic cytoskeletal structure in axons. *Science* 2013;339(6118):452–6.
- [7] Zhang R, Zhang C, Zhao Q, Li D. Spectrin: structure, function and disease. *Sci China Life Sci* 2013;56(12):1076–85.
- [8] Al Mahmud KAH, Hasan F, Khan MI, Adnan A. On the molecular level cavitation in soft gelatin hydrogel. *Sci Rep* 2020;10:1–13.

- [9] Hasan F, Al Mahmud KAH, Khan MI, Patil S, Dennis BH, Adnan A. Cavitation induced damage in soft biomaterials. *Multiscale Sci Eng* 2021;3(1):67–87.
- [10] Khan MI, Hasan F, Mahmud KAH, Adnan A. Recent computational approaches on mechanical behavior of axonal cytoskeletal components of neuron. *A Brief Rev Multiscale Sci Eng* 2020;2(4):199–213.
- [11] Khan MI, Hasan F, Hasan Al Mahmud KA, Adnan A. Domain focused and residue focused phosphorylation effect on tau protein: A molecular dynamics simulation study. *J Mech Behav Biomed Mater* 2021;113:104149. <https://doi.org/10.1016/j.jmbmm.2020.104149>.
- [12] Khan MI, Gilpin K, Hasan F, Hasan Al Mahmud KA, Adnan A. Effect of strain rate on single tau, dimerized tau and tau-microtubule interface: A molecular dynamics simulation study. *J Mech Behav Biomed Mater* 2020.
- [13] Chu J-W, Voth GA. Coarse-grained modeling of the actin filament derived from atomistic-scale simulations. *Biophys J* 2006;90(5):1572–82.
- [14] Matsushita S, Inoue Y, Hojo M, Sokabe M, Adachi T. Effect of tensile force on the mechanical behavior of actin filaments. *J Biomech* 2011;44(9):1776–81.
- [15] Huxley HE, Stewart A, Sosa H, Irving T. X-ray diffraction measurements of the extensibility of actin and myosin filaments in contracting muscle. *Biophys J* 1994. 67. 2411–21. [https://doi.org/10.1016/S0006-3495\(94\)80728-3](https://doi.org/10.1016/S0006-3495(94)80728-3).
- [16] Kojima H, Ishijima A, Yanagida T. Direct measurement of stiffness of single actin filaments with and without tropomyosin by in vitro nanomanipulation. *Proc. Natl. Acad. Sci.* 1994. 91. 12962. LP – 12966. <https://doi.org/10.1073/pnas.91.26.12962>.
- [17] ben-Avraham D, Tirion MM. Dynamic and elastic properties of F-actin: a normal-modes analysis. *Biophys J* 1995;68(4):1231–45.
- [18] Wakabayashi K, Sugimoto Y, Tanaka H, Ueno Y, Takezawa Y, Amemiya Y. X-ray diffraction evidence for the extensibility of actin and myosin filaments during muscle contraction. *Biophys J* 1994;67:2422–35. [https://doi.org/10.1016/S0006-3495\(94\)80729-5](https://doi.org/10.1016/S0006-3495(94)80729-5).
- [19] Higuchi H, Yanagida T, Goldman YE. Compliance of thin filaments in skinned fibers of rabbit skeletal muscle. *Biophys J* 1995;69:1000–10. [https://doi.org/10.1016/S0006-3495\(95\)7975-1](https://doi.org/10.1016/S0006-3495(95)7975-1).
- [20] Isambert H, Venier P, Maggs AC, Fattoum A, Kassab R, Pantaloni D, et al. Flexibility of actin filaments derived from thermal fluctuations. Effect of bound nucleotide, phalloidin, and muscle regulatory proteins. *J Biol Chem* 1995;270(19):11437–44.
- [21] Tsuda Y, Yasutake H, Ishijima A, Yanagida T. Torsional rigidity of single actin filaments and actin-actin bond breaking force under torsion measured directly by in vitro micromanipulation. *Proc Natl Acad Sci* 1996;93(23):12937–42.
- [22] Oda T, Iwasa M, Aihara T, Maeda Y, Narita A. The nature of the globular-to-fibrous-actin transition. *Nature* 2009;457(7228):441–5.
- [23] Pfandtner J, Lyman E, Pollard TD, Voth GA. Structure and dynamics of the actin filament. *J Mol Biol* 2010;396(2):252–63.
- [24] Matsushita S, Inoue Y, Adachi T. Quantitative analysis of extension-torsion coupling of actin filaments. *Biochem Biophys Res Commun* 2012;420(4):710–3.
- [25] Matsushita S, Adachi T, Inoue Y, Hojo M, Sokabe M. Evaluation of extensional and torsional stiffness of single actin filaments by molecular dynamics analysis. *J Biomech* 2010;43(16):3162–7.
- [26] De La Cruz EM, Roland J, McCullough BR, Blanchoin L, Martiel J-L. Origin of twist-bend coupling in actin filaments. *Biophys J* 2010;99(6):1852–60.
- [27] McCullough B, Grintsevich E, Chen C, Kang H, Hutchison A, Henn A, et al. Cofilin-linked changes in actin filament flexibility promote severing. *Biophys J* 2011;101(1):151–9.
- [28] Rebello CA, Ludescher RD. Influence of tightly bound Mg<sup>2+</sup> and Ca<sup>2+</sup>, nucleotides, and phalloidin on the microsecond torsional flexibility of F-actin. *Biochemistry* 1998;37(41):14529–38.
- [29] De La Cruz EM. How cofilin severs an actin filament. *Biophys Rev* 2009;1(2):51–9. <https://doi.org/10.1007/s12551-009-0008-5>.
- [30] Schmolzer KM, Lielog O, Bausch AR. Structural and viscoelastic properties of actin/filamin networks: cross-linked versus bundled networks. *Biophys J* 2009;97(1):83–9.
- [31] Lielog O, Schmolzer KM, Claessens MMAE, Bausch AR. Cytoskeletal Polymer Networks: Viscoelastic Properties are Determined by the Microscopic Interaction Potential of Cross-links. *Biophys J* 2009;96:4725–32. <https://doi.org/10.1016/j.bpj.2009.03.038>.
- [32] Kim Ji, Kwon J, Baek I, Na S. Steered molecular dynamics analysis of the role of cofilin in increasing the flexibility of actin filaments. *Biophys Chem* 2016;218:27–35. <https://doi.org/10.1016/j.bpc.2016.08.002>.
- [33] Deriu MA, Shkurti A, Paciello G, Bidone TC, Morbiducci U, Ficarra E, et al. Multiscale modeling of cellular actin filaments: From atomistic molecular to coarse-grained dynamics. *Proteins Struct Funct Bioinforma* 2012;80(6):1598–609.
- [34] Witek MA, Fung L-W-M. Quantitative studies of caspase-3 catalyzed  $\alpha$ -spectrin breakdown. *Brain Res* 2013;1533:1–15.
- [35] Smith AS, Nowak RB, Zhou S, Giannetto M, Gokhin DS, Papoin J, et al. Myosin IIA interacts with the spectrin-actin membrane skeleton to control red blood cell membrane curvature and deformability. *Proc Natl Acad Sci.* 2018. 115. E4377 LP–E4385. <https://doi.org/10.1073/pnas.1718285115>.
- [36] An X, Lecomte MC, Chasis JA, Mohandas N, Gratzner W. Shear-response of the spectrin dimer-tetramer equilibrium in the red blood cell membrane. *J Biol Chem* 2002;277(35):31796–800.
- [37] Dao M, Li J, Suresh S. Molecularly based analysis of deformation of spectrin network and human erythrocyte. *Mater Sci Eng C* 2006;26(8):1232–44.
- [38] Hoore M, Yaya F, Podgorski T, Wagner C, Gompper G, Fedosov DA. Effect of spectrin network elasticity on the shapes of erythrocyte doublets. *Soft Matter* 2018;14(30):6278–89.
- [39] Law R, Carl P, Harper S, Dalhaimer P, Speicher DW, Discher DE. Cooperativity in forced unfolding of tandem spectrin repeats. *Biophys J* 2003;84(1):533–44.
- [40] Lenne P-F, Raaij AJ, Altmann SM, Saraste M, Hörber JKH. States and transitions during forced unfolding of a single spectrin repeat. *FEBS Lett* 2000;476:124–8.
- [41] Viel A. K-Actinin and spectrin structures: an unfolding family story. *FEBS Lett* 1999;460:394.
- [42] Altmann SM, Grünberg RG, Lenne P-F, Ylänne J, Raaij A, Herbert K, et al. Pathways and intermediates in forced unfolding of spectrin repeats. *Structure* 2002;10(8):1085–96.
- [43] Ortiz V, Nielsen SO, Klein ML, Discher DE. Unfolding a linker between helical repeats. *J Mol Biol* 2005;349(3):638–47.
- [44] Paramore S, Voth GA. Examining the influence of linkers and tertiary structure in the forced unfolding of multiple-repeat spectrin molecules. *Biophys J* 2006;91(9):3436–45.
- [45] Rief M, Pascual J, Saraste M, Gaub HE. Single molecule force spectroscopy of spectrin repeats: low unfolding forces in helix bundles. *J Mol Biol* 1999;286(2):553–61.
- [46] Zhu Q, Asaro RJ. Spectrin Folding versus Unfolding Reactions and RBC Membrane Stiffness. *Biophys J* 2008;94:2529–45. <https://doi.org/10.1529/biophysj.107.119438>.
- [47] Huang C-M, Zhang C, Ho T-Y, Osés-Prieto J, Burlingame AL, Lalonde J, et al.  $\alpha$ II spectrin forms a periodic cytoskeleton at the axon initial segment and is required for nervous system function. *J Neurosci* 2017;37(47):11311–22.
- [48] Barabas FM, Masullo LA, Bordenave MD, A. Giusti S, Unsain N, Refojo D, et al. Automated quantification of protein periodic nanostructures in fluorescence microscopy images: abundance and regularity of neuronal spectrin membrane-associated skeleton. *Sci Rep* 2017;7(1). <https://doi.org/10.1038/s41598-017-16280-x>.
- [49] Han B, Zhou R, Xia C, Zhuang X. Structural organization of the actin-spectrin-based membrane skeleton in dendrites and soma of neurons. *Proc Natl Acad Sci* 2017;114(32):E6678–85.
- [50] Koskinen M, Hotalainen P. Measuring F-actin properties in dendritic spines. *Front Neuroanat* 2014;8:74.
- [51] Sidenstein SC, D'Este E, Böhm MJ, Danzl JG, Belov VN, Hell SW. Multicolor multilevel STED nanoscopy of actin/spectrin organization at synapses. *Sci Rep* 2016;6:26725. <https://doi.org/10.1038/srep26725>.
- [52] Abouelezz A. The Structure and Dynamics of the Actin Cytoskeleton in the Axon Initial Segment. *Diss Sch Dr Ad Sanit Investig Univ Hels* 2020.
- [53] Bär J, Kobler O, Van Bommel B, Mikhaylova M. Periodic F-actin structures shape the neck of dendritic spines. *Sci Rep* 2016;6:1–9.
- [54] Zhong G, He J, Zhou R, Lorenzo D, Babcock HP, Bennett V, et al. Developmental mechanism of the periodic membrane skeleton in axons. *Elife*. 2014. 3. e04581. <https://doi.org/10.7554/eLife.04581>.
- [55] Costa AR, Pinto-Costa R, Sousa SC, Sousa MM. The regulation of axon diameter: from axonal circumferential contractility to activity-dependent axon swelling. *Front Mol Neurosci* 2018;11:319.
- [56] Leite S, Sampaio P, Sousa V, Nogueira-Rodrigues J, Pinto-Costa R, Peters L, et al. The actin-binding protein  $\alpha$ -adducin is required for maintaining axon diameter. *Cell Rep* 2016;15(3):490–8.
- [57] Leite SC, Sousa MM. The neuronal and actin commitment: Why do neurons need rings? *Cytoskeleton* 2016;73:424–34.
- [58] Qu Y, Hahn I, Webb SED, Pearce SP, Prokop A, Forscher P. Periodic actin structures in neuronal axons are required to maintain microtubules. *Mol Biol Cell* 2017;28(2):296–308.
- [59] Koshino I, Mohandas N, Takakuwa Y. Identification of a novel role for dematin in regulating red cell membrane function by modulating spectrin-actin interaction. *J Biol Chem* 2012;287(42):35244–50.
- [60] Wang G, Simon DJ, Wu Z, Belsky DM, Heller E, O'Rourke MK, et al. Structural plasticity of actin-spectrin membrane skeleton and functional role of actin and spectrin in axon degeneration. *Elife*. 2019. 8. e38730.
- [61] Dubey S, Bhemre N, Bodas S, Veer S, Ghose A, Callan-Jones A, et al. The axonal actin-spectrin lattice acts as a tension buffering shock absorber. *Elife* 2020;9:e51772.
- [62] Wu Y-T, Adnan A. Damage and failure of axonal microtubule under extreme high strain rate: an in-silico molecular dynamics study. *Sci Rep* 2018;8:12260.
- [63] Zhang Y. I-TASSER server for protein 3D structure prediction. *BMC Bioinf* 2008;9:40.
- [64] Castro T, Munteanu F-D, Cavaco-Paulo A. Electrostatics of tau protein by molecular dynamics. *Biomolecules* 2019;9(3):116. <https://doi.org/10.3390/biom9030116>.
- [65] Battisti A, Tenenbaum A. Molecular dynamics simulation of intrinsically disordered proteins. *Mol Simul* 2012;38(2):139–43.
- [66] Plimpton S. Fast parallel algorithms for short-range molecular dynamics. *J Comput Phys* 1995;117:1–19. <https://doi.org/10.1006/jcph.1995.1039>.
- [67] Jorgensen WL, Maxwell DS, Tirado-Rives J. Development and testing of the OPLS all-atom force field on conformational energetics and properties of organic liquids. *J Am Chem Soc* 1996;118(45):11225–36. <https://doi.org/10.1021/ja9621760>.
- [68] Bernardes CES, Joseph A. Evaluation of the OPLS-AA force field for the study of structural and energetic aspects of molecular organic crystals. *J Phys Chem A* 2015;119(12):3023–34.

- [69] Marrink SJ, Risselada HJ, Yefimov S, Tieleman DP, De Vries AH. The MARTINI force field: coarse grained model for biomolecular simulations. *J Phys Chem B* 2007;111:7812–24.
- [70] Narita A, Oda T, Maéda Y. Structural basis for the slow dynamics of the actin filament pointed end. *EMBO J* 2011;30:1230–7. <https://doi.org/10.1038/emboj.2011.48>.
- [71] Murakami K, Yasunaga T, Noguchi TQP, Gomibuchi Y, Ngo KX, Uyeda TQP, et al. Structural basis for actin assembly, activation of ATP hydrolysis, and delayed phosphate release. *Cell* 2010;143(2):275–87. <https://doi.org/10.1016/j.cell.2010.09.034>.
- [72] Moon RT, McMahon AP. Generation of diversity in nonerythroid spectrins. Multiple polypeptides are predicted by sequence analysis of cDNAs encompassing the coding region of human nonerythroid alpha-spectrin. *J Biol Chem* 1990;265(8):4427–33.
- [73] Nagase T, Ishikawa K, Nakajima D, Ohira M, Seki N, Miyajima N, et al. Prediction of the coding sequences of unidentified human genes. VII. The complete sequences of 100 new cDNA clones from brain which can code for large proteins in vitro. *DNA Res* 1997;4:141–50.
- [74] C. Rycroft. Voro++: a three-dimensional Voronoi cell library in C++. United States: 2009. <https://doi.org/10.2172/946741>.
- [75] Stukowski A. Visualization and analysis of atomistic simulation data with OVITO—the Open Visualization Tool. *Model Simul Mater Sci Eng* 2010;18(1):015012. <https://doi.org/10.1088/0965-0393/18/1/015012>.
- [76] Robertson MJ, Tirado-Rives J, Jorgensen WL. Improved peptide and protein torsional energetics with the OPLS-AA force field. *J Chem Theory Comput* 2015;11(7):3499–509. <https://doi.org/10.1021/acs.jctc.5b00356>.
- [77] Kaminski GA, Friesner RA, Tirado-Rives J, Jorgensen WL. Evaluation and reparametrization of the OPLS-AA force field for proteins via comparison with accurate quantum chemical calculations on peptides. *J Phys Chem B* 2001;105(28):6474–87. <https://doi.org/10.1021/jp003919d>.
- [78] Battisti A, Ciasca G, Grottesi A, Bianconi A, Tenenbaum A. Temporary secondary structures in tau, an intrinsically disordered protein. *Mol Simul* 2012;38(7):525–33.
- [79] Berro J, Michelot A, Blanchoin L, Kovar DR, Martiel J-L. Attachment conditions control actin filament buckling and the production of forces. *Biophys J* 2007;92(7):2546–58.